



## Regression modelling of radiant fluxes on different view factors under shading in a densely built environment

Alan Lai, Yu Ting Kwok, Minjung Maing & Edward Ng

To cite this article: Alan Lai, Yu Ting Kwok, Minjung Maing & Edward Ng (2017): Regression modelling of radiant fluxes on different view factors under shading in a densely built environment, Architectural Science Review, DOI: [10.1080/00038628.2017.1409614](https://doi.org/10.1080/00038628.2017.1409614)

To link to this article: <https://doi.org/10.1080/00038628.2017.1409614>



Published online: 08 Dec 2017.



Submit your article to this journal [↗](#)



View related articles [↗](#)



View Crossmark data [↗](#)



# Regression modelling of radiant fluxes on different view factors under shading in a densely built environment

Alan Lai<sup>a</sup>, Yu Ting Kwok<sup>a</sup>, Minjung Maing<sup>b</sup> and Edward Ng<sup>a,c,d</sup>

<sup>a</sup>School of Architecture, The Chinese University of Hong Kong, Hong Kong, People's Republic of China; <sup>b</sup>Faculty of Architecture, The University of Hong Kong, Hong Kong, People's Republic of China; <sup>c</sup>Institute of Environment, Energy and Sustainability, The Chinese University of Hong Kong, Hong Kong, People's Republic of China; <sup>d</sup>Institute of Future Cities, The Chinese University of Hong Kong, Hong Kong, People's Republic of China

## ABSTRACT

The exchange of radiant fluxes between different surfaces in an outdoor environment can be described with an enclosure theory. It provides a physical understanding of the relationship between different surfaces and consequent radiant fluxes within an enclosure, which is constructed by including surfaces of building façades and an imaginary surface of sky dome. Radiant fluxes on a surface can be expressed as linear combinations of view factors. This study examines the linear dependencies of urban radiant fluxes on view factors, namely Sunlit View Factor (SLVF), Green View Factor (GNVF), and Sky View Factor (SVF), using an empirical regression analysis. Results revealed a simple and linear correlation between view factors and outdoor radiant fluxes. As such, a quick estimation of the potential increase in the outdoor mean radiant temperature in relation to neighboring built environments can be achieved, and industry guidelines for designing thermally comfortable open spaces can be formulated accordingly.

## ARTICLE HISTORY

Received 20 November 2016  
Accepted 21 November 2017

## KEYWORDS

Urban morphology; radiant fluxes; Sky View Factor (SVF); Sunlit View Factor (SLVF); Green View Factor (GNVF)

## Introduction

In recent years, considerable concern has arisen over the importance of designing open spaces for better human thermal comfort. A thermally comfortable open space promotes public health in cities by encouraging people to go outdoors for various activities (Hakim et al. 1998; Lin, Matzarakis, and Hwang 2010; Lin et al. 2012; Tan, Wong, and Jusuf 2013). Objective assessments of the comfort level of an open space is closely associated with four fundamental physical parameters: air temperature, relative humidity, wind speed, and mean radiant temperature (MRT) (Fanger 1972), among which MRT is the only physical parameter that directly relates to the radiant energy exchange between the human body and ambient environments which the body is exposed to (ASHRAE 2013). It is thus widely employed for the calculation of thermal assessment indices, such as Physiological Equivalent Temperature (Höppe 1999) and Universal Thermal Climate Index (Jendritzky, de Dear, and Havenith 2012). Moreover, the radiant energy exchange involves both the long-wave and short-wave radiant fluxes. Therefore, MRT is the essential physical parameter linking long-wave and short-wave radiative energy transfers to human thermal comfort and ambient man-made open spaces.

The MRT can be obtained by several means with the aid of computer software and field measurements of radiant fluxes and globe temperature. The most accurate method to determine MRT, *integral radiation measurement*, requires the measurement of short-wave and long-wave radiant fluxes that affect the human body in three dimensions (Thorsson et al. 2007).

The three-dimensional radiant fluxes, both short-wave and long-wave, are represented by fluxes from the four cardinal directions, as well as the upper and lower hemispheres. Therefore, to simulate the reception of radiative energy fluxes on the human body, the measuring instrument should consist of six net radiometer sensors facing all six directions. The transfer of radiative energy between the human body (i.e. surfaces of the sensors) and the outdoor environment can then be described based on the enclosure theory, or the net radiation method (Mbiok and Weber 2000; Howell, Menguc, and Siegel 2010), for each direction. Such energy transfer depends on the relative positions and orientations of different surfaces, for example the human skin (i.e. surfaces of the sensors) and the building façades in the outdoor environment. The view factor is a parameter describing the geometric relationships between different surfaces with respect to radiative energy transfer. Therefore, the effects of view factors on determining MRT are fundamentally important.

Many have investigated the relationship between MRT and Sky View Factor (SVF) (Hamdi and Schayes 2007; Lin, Matzarakis, and Hwang 2010; Krüger, Minella, and Rasia 2011; Tan, Wong, and Jusuf 2013; Lee, Mayer, and Schindler 2014; Lai, Maing, and Ng 2017). SVF is a widely used dimensionless quantity that describes the degree of obstruction within a complex urban environment (Oke 1988; Unger 2009; Lin, Matzarakis, and Hwang 2010, 2012; Tan, Wong, and Jusuf 2013). As its name suggests, SVF is the fraction of sky visible from an observation point, where an SVF of 1 means a completely unobstructed sky view. Several studies have revealed that a higher MRT can be attributed

to a higher SVF due to the exposure of direct sunlight under sunny conditions (Krüger, Minella, and Rasia 2011; Tan, Wong, and Jusuf 2013; Lee, Mayer, and Schindler 2014). Tan, Wong, and Jusuf (2013) have shown a linear correlation between MRT and SVF at two sites with 10 and 7 sample points, and the coefficients of determination ( $R^2$ ) reported were 0.61 and 0.32, respectively. In particular, Lee, Mayer, and Schindler (2014) employed the SVF for the 'southern part of upper half space' (SVF<sub>90–270</sub>) instead of the conventional 'whole upper half space' (SVF<sub>0–360</sub>), to give an improved correlation MRT and SVF, from an  $R^2$  of 0.57–0.77. This may be explained by the larger overlapping area between the sun path and the southern sky view. Moreover, Krüger, Minella, and Rasia (2011) investigated the relationship between SVF and the temperature difference between measured MRT and ambient air temperature ( $\Delta\text{MRT} - T$ ). A positive correlation with  $R^2 = 0.57$  was found using a sample size of 14 points, owing to the strong dependence of MRT on direct solar radiation. In brief, these studies suggested that a higher SVF would cause a higher MRT by allowing more direct solar radiation onto open spaces. In other words, these studies regarded SVF as a degree of openness of the outdoor environment to direct solar radiation, and neglected, by first principles, the physical meaning of 'view factor' in the radiative energy transfer.

Although previous studies have been performed to examine the effect of SVF on MRT, these studies only focused on the shading effect of SVF on reducing daytime MRT by blocking direct sunlight. Few have been able to establish a direct and empirical relationship between radiant fluxes and SVF/view factors of other surfaces by field measurement. This study is an attempt to supplement the findings of earlier studies. Similar to the precedent studies, this paper focuses on how view factors affect outdoor thermal comfort. However, it differs by evaluating empirically how view factors of the sky, sunlit areas, and greenery areas simultaneously affect the variations in radiant fluxes that constitute to the MRT of open spaces. The methodology adopted takes reference from the empirical study by Wong and Jusuf (2010), in which linear regression analysis was used to study the effect of SVF on air temperature. The goal of this study is to evaluate empirically the linear dependencies of urban radiant fluxes on several view factors casted by a densely built environment. Therefore, the objectives of the study can be summarized as follows:

1. To determine empirically whether view factors of the urban environment are linearly correlated to radiant fluxes and
2. To obtain the regression equation relating view factors of the urban environment to radiant fluxes.

### Urban environment and view factors

Urban outdoor environments can be geometrically defined by building façades and outdoor objects, forming an irregular enclosure of  $N$ -surface areas possessing their own surface temperatures (Howell, Menguc, and Siegel 2010; Michael 2013). The magnitude of radiative heat transfer between any two surfaces of this  $N$ -surface enclosure depends on their corresponding surface temperatures, relative surface geometry, and orientations. The view factor is a parameter to represent the relative geometric configurations between any two surfaces. It is defined

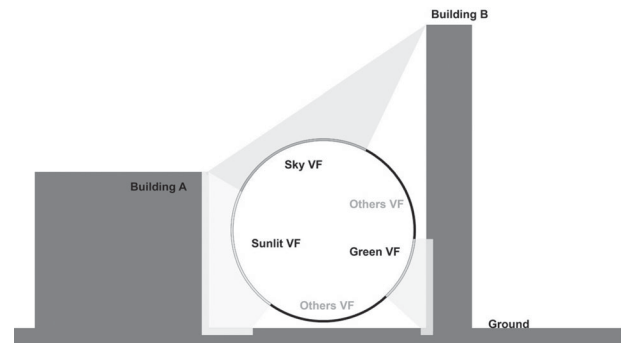


**Figure 1.** Schematic diagram of view factors as visual projections of built environment on spherical surfaces in sectional view.

to account for the fraction of radiation energy emitted and reflected by an intercepting surface which one can 'view' from the first surface.

Refer to Figure 1 which shows a spherical surface represented by a full circle in the 2D schematic diagram. The amount of radiation energy from the sky that this surface receives is proportional to the amount of sky view it perceives. The amount of sky view, i.e. SVF, can be calculated by summarizing the projected area of sky view on that spherical surface, which is represented by the blue arc on the circle in Figure 1. Similarly, the view factors of other interested areas of the built environment can therefore be obtained by summarizing the corresponding projected areas on the spherical surface. For example, the sunlit surface and the greenery area, including trees and vertical greening on buildings, are projected onto the spherical surface as in Figure 1. As a result, view factors of any surfaces of interest within a built environment can be evaluated using the same way.

### Fisheye photographs and view factors

If only half of the spherical surface is considered, a hemispherical surface is thus formed and represented by the semicircular arc in Figure 2(a). The view factor of any surface  $S$  can be simply obtained by applying equiangular projection (Steyn 1980) on a 'planar surface', which can be represented in a 2D schematic diagram by a coloured arc in Figure 2(b). As a result, the projected image,  $S'$  of surface  $S$  on the 'planar surface', could be presented as ultra-wide-angle photographs (fisheye photographs) as shown in Figure 2(c). The view factor,  $F_{O-S}$  of that surface  $S$  when viewed from an object  $O$ , for example the radiation sensor, at the centre of the hemispherical surface could therefore be computed with Equation (1) as given by Steyn (1980).

$$F_{O-S} = \frac{1}{\pi r_O^2} \int_S \cos \beta_1 \cos \beta_2 dS, \quad (1)$$

where  $\beta_1$  is the polar angle formed between surface normal  $\hat{n}_O$  and the reference line joining elemental areas of surface  $O$  and  $S$ ;  $\beta_2$  is the polar angle formed between surface normal  $\hat{n}_S$  and the reference line joining elemental areas of surface  $O$  and  $S$ ;  $\pi r_O^2$  is the area of the circle, which is equal to the base of the hemispherical surface formed by the fisheye photograph.

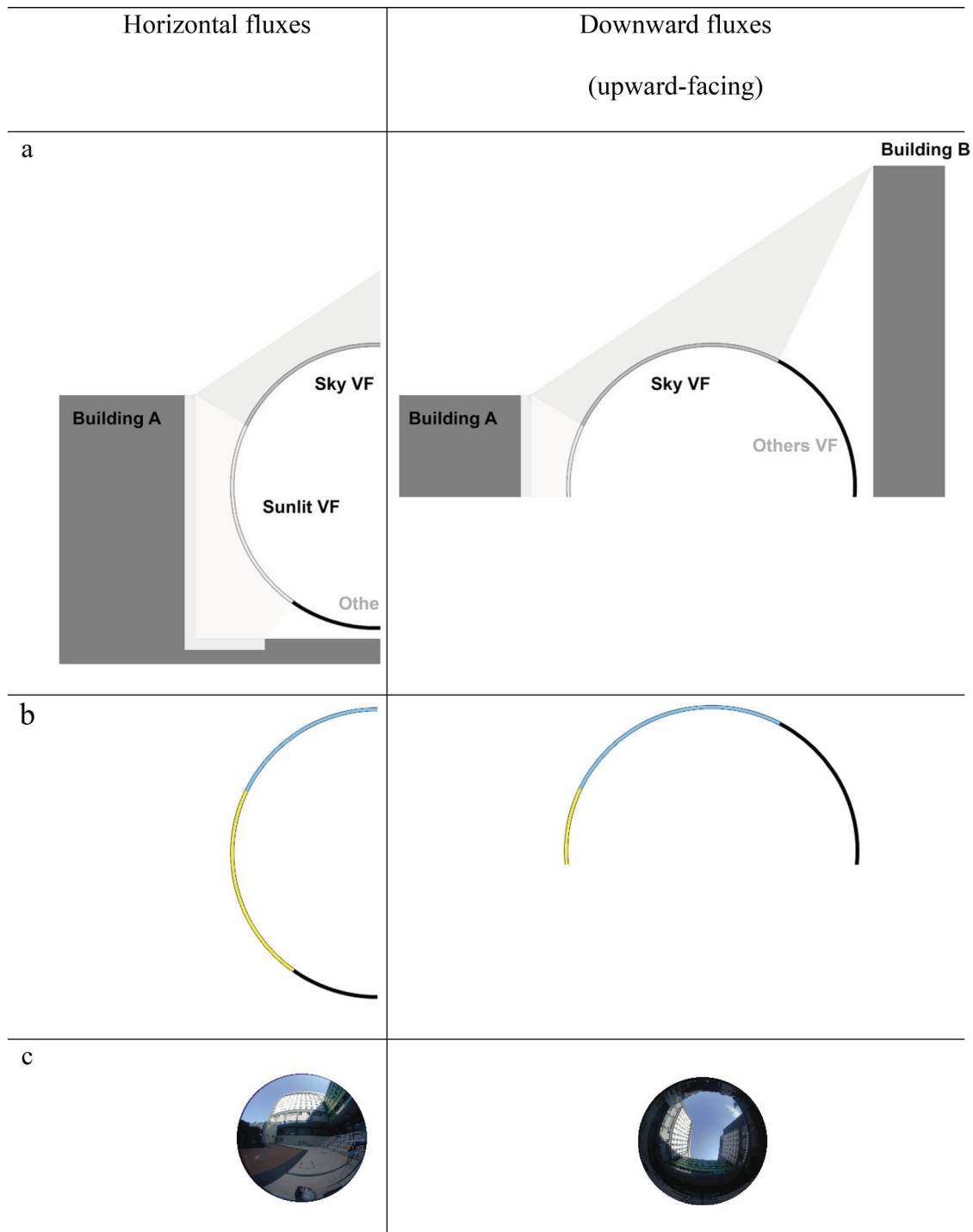


**Figure 2.** Relationship between radiant fluxes and view factors in sectional view. (a) The photons (visible or non-visible light) leave from built environment and incident on the spherical surfaces; (b) The total amount of radiant fluxes (photons), which incident on the hemispherical surfaces represented by the arc, depends on different view factors of different surfaces. (c) The fisheye photographs record different view factors through visible light as an example.

Moreover, using fisheye photographs of the urban environment, the view factor of a certain surface could be determined by further applying Nusselt's 'Unit Sphere Method' as given in Equation (2) (Howell, Menguc, and Siegel 2010).

$$F_{O-S} = \frac{1}{\pi r_0^2} \int_{S''} dS'' \quad (2)$$

where  $S''$  is the equiangular projection of area  $S$  captured by in the fisheye photograph.

### Radiant fluxes and view factors

As a generalization, considering the radiation sensor as object  $O$  at the centre of the hemispherical surface, the incidental irradiation it receives,  $G_O$ , is the sum of irradiation intercepted by area  $A_O$  and emitted by all other surfaces within the hemispherical enclosure.  $G_O$  can thus be defined by Equation (3) as follows:

$$A_O G_O = \sum_{i=1}^N A_i F_{i-O} J_i \quad (3)$$

where  $F_{i-O}$  is the view factor, defined as the fraction of radiant energy leaving from the  $i$ th surface  $A_i$  and reaching the object  $O$  with area  $A_O$ , and  $J_i$  is the radiosity, which is the sum of emitted and reflected radiant energy leaving from the  $i$ th surface. If using the Reciprocity rule as in Equation (4),

$$A_O F_{O-i} = A_i F_{i-O}, \quad (4)$$

then Equation (3) becomes:

$$G_O = \sum_{i=1}^N F_{O-i} J_i, \quad (5)$$

where  $F_{O-i}$  is the view factor, defined as the fraction of radiant energy leaving from the surface  $A_O$  and reaching the surface  $A_i$ . If there are three kinds of surfaces,  $S_1$ ,  $S_2$  and  $S_3$ , which are dominant or more significant in the radiative energy transfer of the outdoor built environment, then Equation (5) would give:

$$G_O = J_1 F_{O-1} + J_2 F_{O-2} + J_3 F_{O-3} + \dots, \quad (6)$$

where  $F_{O-1}$  is the view factor, defined as the fraction of radiant energy leaving from the surface  $A_O$  and reaching the surface  $S_1$ , and so on. And these view factors are computed using Equation (1) or (2). It should be noted that the irradiation  $G_O$  on object  $O$ , for example the radiation sensor, can be regarded as a linear combination of view factors of some surfaces  $S_i$  viewed by object  $O$  if only radiation energy is considered.

### Types of view factors

The three view factors casted by the urban environment, namely SVF, Sunlit View Factor (SLVF), and Green View Factor (GNVF), to be mentioned in this paper are described below.

The SVF, denoted by  $\Psi_{sky}$ , is a ratio between the radiation received (or emitted) by a planar surface and the radiation emitted (or received) from the entire hemispheric environment (Watson and Johnson 1987). SVF represents the visible sky that might scatter solar radiation and emit fewer long-wave fluxes due to its lower effective temperature. SVF is a dimensionless quantity, ranging from zero to unity, to describe the degree of obstruction by the urban canyon (Oke 1988). As its name suggests, SVF is the fraction of sky dome that can be viewed from a particular point within the canyon (Erell, Pearlmutter, and Williamson 2010). It is widely used to define complex urban geometries (Johnson and Watson 1984; Unger 2009). Besides, it has often been associated with the cooling rate of the city at night (Chapman, Thornes, and Bradley 2001).

Similar to SVF, SLVF, denoted by  $\Psi_{sunlit}$ , is the fraction of sunlit building façades that can be viewed from a particular point within the urban environment. SLVF is also a dimensionless quantity from zero to unity. Theoretically, SLVF should also be important when determining the radiative energy exchange for an urban context as sunlit surfaces might reflect more short-wave fluxes and emit more long-wave fluxes compared to shaded surfaces. It should be associated with the warming effects of a city in the daytime. Therefore, SLVF is chosen for investigation in this study.

The GNVF, denoted by  $\Psi_{green}$ , is the fraction of greenery area of the built environment that can be viewed from a particular

observation point within the built environment. Similarly, GNVF varies from zero to unity. GNVF represents the greenery feature in the built environment that might absorb certain portions of solar radiation for photosynthesis and emit fewer long-wave fluxes due to its water content of higher specific heat capacity. It could be associated with the shadowing effect of trees, or cooling effect (if any) of other greenery features, such as trees, vertical greening, grass lawns, etc.

With reference to Equations (5) and (6), the irradiation  $G_O$ , defined as the sum of radiation energy from different surfaces approaching the radiation sensor, could also be expressed as the linear combination of view factors of different surfaces, with their respective radiosities incorporated into their corresponding coefficients. However, such radiosities are generally unknown or hard to be measured for each differential isothermal surface in the built environment. Therefore, the irradiation  $G_O$  on the sensor would be measured instead and regressed against predictors of view factors. In this way, the empirical correlation between radiant fluxes and view factors could be evaluated for the outdoor built environment by multiple regression analysis.

### The use of multiple linear regression analysis

The multiple linear regression analysis was adopted to quantify empirically the linear dependencies of measured radiant fluxes on different view factors. In fact, the linear dependence of radiant fluxes on view factors is supported by the theory of radiative energy transfer within an enclosure as the radiant fluxes incident on the sensors could be expressed as a linear combination of view factors of surfaces in the built environment as in Equation (5). This theoretical relationship not only justified the use of a linear model but also provided the basis, which is called 'response schedule' (Freeman 2009), for drawing causal inferences from an observational study. Therefore, in this study, empirical linear relations were examined and multiple linear regressions were performed on long-wave and short-wave radiant fluxes with the view factors as predictors. The linear mathematical relation of multiple linear regression is given in Equation (7):

$$\bar{Y} = b_1 X_1 + b_2 X_2 + b_3 X_3 + b_4 X_4 + b_0, \quad (7)$$

where  $\bar{Y}$  is  $L_i$  for measured long-wave directional radiant fluxes and  $K_i$  for measured short-wave directional radiant fluxes;  $X_1 = \Psi_{sky}$  which is SVF representing the Sky View Factor;  $X_2 = \Psi_{sunlit}$  which is SLVF representing the Sunlit View Factor;  $X_3 = \Psi_{green}$  which is GNVF representing the Green View Factor;  $X_4$  is an additional predictor for adjusting the weather and climatic conditions as reference background information:  $L_o$  for long-wave fluxes in long-wave model and  $= K_o$  for diffuse solar radiation in short-wave model;  $b_1$  is the estimate of the parameter of the model for SVF;  $b_2$  is the estimate of the parameter of the model for SLVF;  $b_3$  is the estimate of the parameter of the model for GNVF;  $b_4$  is the estimate of the parameter of the model for either  $L_o$  or  $K_o$ ;  $b_0$  is the estimate of the intercept, the value of  $Y$  when all  $X_i$  equal zero.

## Methodology

### Measurement of directional radiant fluxes

The aim of this study is to evaluate empirically the linear dependencies of urban radiant fluxes on several view factors within a densely built environment. The three-dimensional directional short-wave and long-wave radiant fluxes were measured by the net radiometers (Kipp & Zonen, CNR4), as specified in Table 1. A set of three CNR4 net radiometers were mounted on a tripod for measuring different directional radiant fluxes incident on the sensor surfaces from the six directions, namely from the sky dome (downward fluxes), from the four cardinal horizontal directions (northerly, easterly, southerly, and westerly), and from the ground (upward fluxes). Measurements of radiant fluxes were taken at a height of approximately 1.5 m above ground level

**Table 1.** Specification of the net radiometers.

Specifications	CNR4 Net Radiometer
Operating temperature	−40 to +80 °C
Environmental	0–100% RH (Relative Humidity)
Spectral range	300–2800 nm short-wave 4.5–42 μm long-wave
Field of view	180° short-wave upper sensor 150° short-wave lower sensor 180° long-wave upper sensor 150° long-wave lower sensor

Note: The logging interval is 10 s each and the measured radiant fluxes were smoothed out using 5-min mean value at 15:00, 15:15, 15:30, and 15:45.

in the open spaces. Measured fluxes affected by the direct sunlight incident on the sensors at the time of measurement were excluded from the regression analysis.

### Study area

The field measurement of radiant fluxes due to ambient built environments were performed in Hong Kong between June and October 2015 in nine different open spaces as shown in Figure 3: (A) in between commercial skyscrapers and residential buildings on 4 June 2015; (B) within the playground area next to a greenery slope in a newly built public residential estate with tall buildings on 15 June 2015; (C) a courtyard and playground area with vertical greening on 15 June and on 5 September 2015; (D) a podium bounded by tall private residential buildings on 29 June 2015; (E) a courtyard area enclosed by short public residential buildings on 7 August 2015; (F) a courtyard area within a university campus on 15 September 2015; (G) a podium enclosed by public residential buildings on 24 September 2015; (H) a courtyard area bounded by a C-shaped building within a university campus on 25 September 2015; (I) in a commercial area bounded by office buildings with curtain walls on 16 October 2015. The measurements were taken on days of clear sky and under shaded conditions to avoid the dominant effect of beam solar radiation on the net radiometers, such that the effect of view factors of the built environment on measured radiant fluxes incident on the

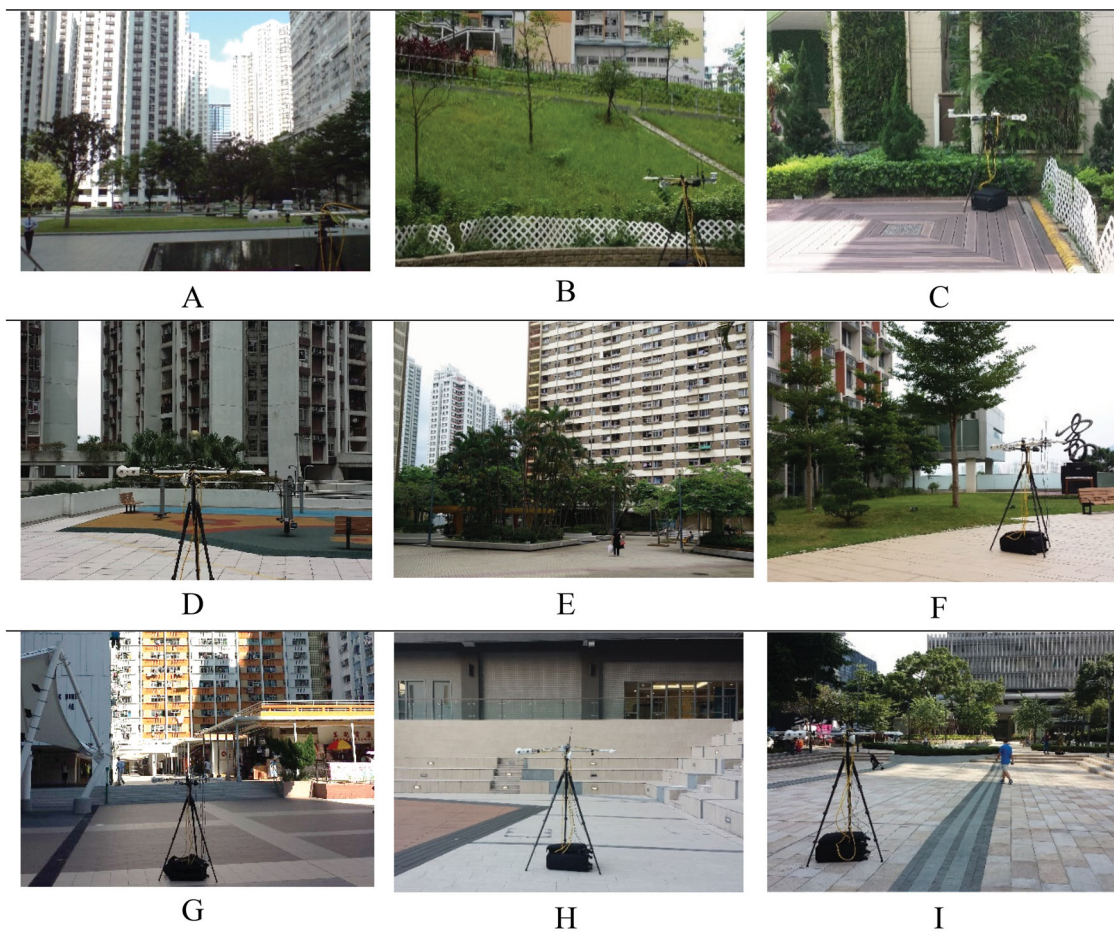


**Figure 3.** Sites photos for the nine different open spaces.

**Table 2.** Description of measurement points.

Site	Description of open spaces	No. of points	Date
A	Open space in-between commercial and residential buildings	A1, A2	June 4
B	Playground area with greenery slope aside in a newly built public residential estate consists of tall buildings	B1, B2	June 15, Sept 5
C	Courtyard and playground area with vertical greening	C	June 15
D	Podium bounded by private residential buildings	D	June 29
E	Courtyard area enclosed by public residential buildings	E	Aug 7
F	Courtyard in a university	F	Sept 15
G	Podium enclosed by public residential buildings	G	Sept 24
H	Courtyard area bounded by C-shaped student hostel in university	H	Sept 25
I	Podium enclosed by Public Housing buildings	I1, I2, I3, I4	Oct 16

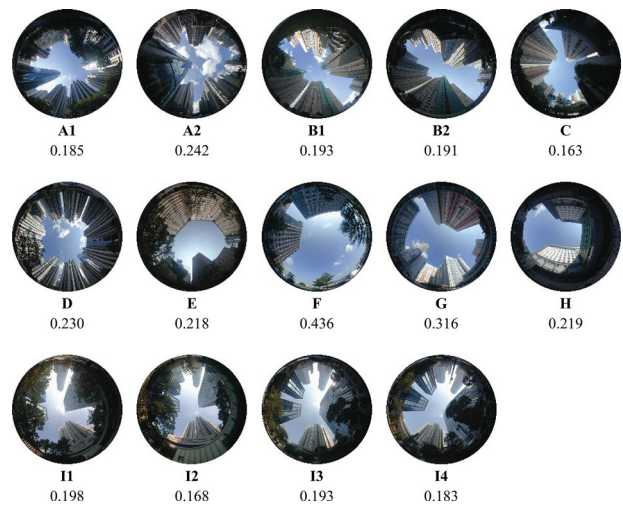
net radiometers could be isolated. Table 2 summarizes the measurement locations in Hong Kong. A total of 14 measurement points were obtained.

### Measurement of view factors with fisheye photographs

The view factor of any surface of the urban environment viewed from the perspective of the net radiometer sensors can be recorded by taking ultra-wide-angle photographs with the camera (Nikon Coolpix 800) equipped with the lens (Nikon fisheye lens FC-E8 0.21x) of a 183-degree coverage. The camera was put alongside the sensors at a height of around 1.5 m above ground level for six directions for every 15-min interval from 15:00 to 16:00 on each day of measurement. Taking the SVF as an example, the conventional SVF images commonly found in literature, denoted as  $SVF_{\text{downward}}$  in this study, were recorded with the ultra-wide-angle lens facing upwards in order to capture the downward visible photons. This is analogous to the corresponding net radiometer sensor with the glass dome facing upwards measuring the downward fluxes, denoted as either  $L_{\text{downward}}$  for downward long-wave fluxes or  $K_{\text{downward}}$  for downward short-wave fluxes in this study. Besides this traditional SVF for downward fluxes, horizontal SVF images were also captured for radiant fluxes from the four cardinal directions: namely easterly, southerly, westerly, and northerly. Images facing downwards have not been included in the study, since they do not capture any sky view. The fisheye photographs taken facing upwards for each measuring points are shown in Figure 4. Together with SVF from five directions, the values of SLVF and GNVF from five directions were extracted from the images and correlated to either long-wave or short-wave radiant fluxes. The summary of the three view factors obtained at measuring point I4 is shown in Figure 5.

### Background climatic conditions on days of measurement

The measurements were taken on days of clear sky and under shading to avoid the dominant effect of beam solar radiation on the net radiometers, so as to truly examine the effect of view factors of built environment on measured radiant fluxes incident on the net radiometers. Besides, the regression models

**Figure 4.** Overview of fisheye photographs that taken with fisheye lens facing upward capturing downward photons for the 14 measurement points.

Direction	Original	SVF	SLVF	GnVF
Downward D		 0.183	 0.015	 0.379
Northerly N		 0.153	 0.084	 0.164
Southerly S		 0.083	 0.021	 0.312
Westerly W		 0.127	 0.098	 0.196
Easterly E		 0.088	 0.050	 0.296

**Figure 5.** Summary of different view factor values from five directions for measurement point I4 at 15:45 as an example that similar to other measurement points.

included additional predictors representing the meteorological conditions of the days of measurement for appropriate climatic adjustments. For the model of long-wave radiant fluxes, an additional predictor, reference background long-wave fluxes  $L_o$ , was used to adjust different meteorological conditions of the days of measurement. This *reference background long-wave fluxes*  $L_o$  was calculated from the *reference air temperature*  $T_o$  by using Stefan–Boltzmann law, i.e.  $L_o = \sigma T_o^4$ , assuming the emissivity of air

as unity (The actual effective emissivity of air on the day of measurement was not measured and not of interest in this study. Also, the effective emissivity of air would be absorbed automatically in the coefficient of  $L_0$  in the regression model.). Nonetheless, the *reference air temperature*  $T_0$  was taken from the Manned Weather Station (22°18'07"N, 114°10'27"E) of the Hong Kong Observatory. Similar to the long-wave model, the short-wave model would include the fourth predictor, the diffuse sky radiation  $K_0$ , in order to adjust for different meteorological conditions. This diffuse sky radiation,  $K_0$ , was extracted from Kau Sai Chau (KSC) Automatic Weather Station (22°22'13"N, 114°18'45"E) of the Hong Kong Observatory. These climatic data provided background information to be used for adjusting the calculation of radiant fluxes on the days of measurement in the multiple regression analysis.

### The regression model

The *all-possible-regressions selection procedure*, requiring the fit of all regression equations taking into account of one candidate predictor, two candidate predictors, and so on (Montgomery and Peck 1982), was adopted for the model building of both the long-wave or short-wave radiant fluxes model. For either of the two models, there would be  $2^4 = 16$  possible regression equations including the intercept  $\beta_0$ , as there are  $k = 4$  candidate predictors. The one regression equation with only the intercept term  $\beta_0$ , i.e. without any one of the four predictors, was omitted. The remaining 15 equations were assessed based on some suitable criteria (Pardoe 2012), and the 'best' regression was selected as the final model for long-wave and short-wave radiant fluxes. Three model selection criteria were used:

- Adjusted  $R^2$ : larger values of adjusted  $R^2$  indicate better-fitting models.
- Akaike Information Criterion (AIC): smaller values indicate better-fitting models (Sakamoto, Ishiguro, and Kitagawa 1987).
- Bayesian Information Criterion (BIC): smaller values indicate better-fitting models (Schwarz 1978).

Based on these three criteria, the model with the largest adjusted  $R^2$  value and the smallest of AIC and BIC values were selected as the final model.

## Results

The results of this study on the dependencies of radiant fluxes on the three aforementioned view factors, namely SLVF, GNVF, and SVF, are presented.

### Observations of surface temperature from thermal images

The radiant fluxes within open spaces could be attributed to the view factors of ambient surfaces. First, a larger SLVF could cause stronger long-wave radiant fluxes to exist within an open space. Figure 5(a, b, e, and f) show higher surface temperatures on sunlit concrete surfaces than their non-sunlit counterparts, indicating that they emit stronger long-wave radiant fluxes. Taking Figure 5(b) as an example, the surface temperature difference

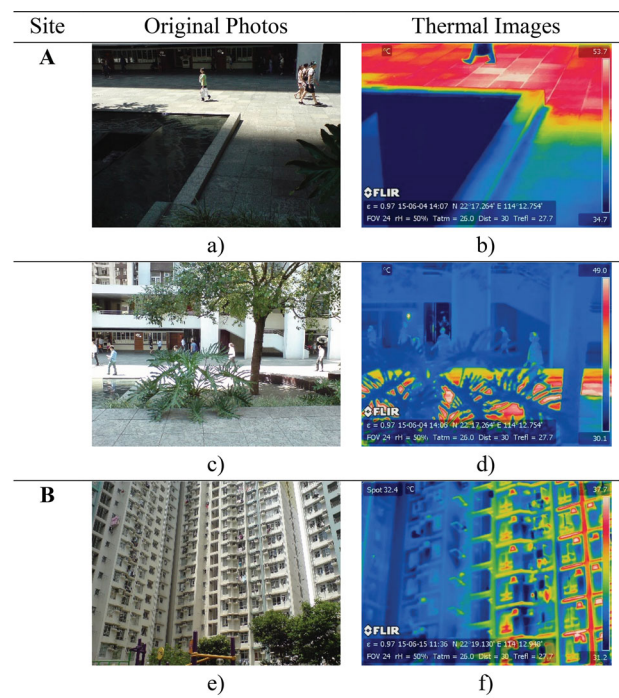


**Figure 6.** Thermal images of surface temperatures at open spaces taking Site A and B as an example.

recorded was up to 10 K between the sunlit concrete ground area and its non-sunlit counterpart during the measurement period in the afternoon. Whereas in Figure 5(f), the sunlit portion of the building façade was found to have a surface temperature 3–4 K higher than the non-sunlit part. These thermal images supported the statement that the higher the SLVF, the larger the amount of long-wave radiant fluxes emitted. In addition, as typical values of emissivity for concrete range from 0.88 to 0.95 (Butcher 1999; Çengel 2003; Rathore and Kapuno 2011), the surface temperatures obtained from the thermal images would only be conservative estimates when calculated using an emissivity set to the largest possible value of 0.95. This means that the effect of SLVF on long-wave radiant flux emissions may well be larger than that reported.

Secondly, a larger GNVF could reduce the amount of strong long-wave radiant fluxes emitted by sunlit concrete surfaces reaching the human body in an open space. In Figure 5(d), the blockage of strong long-wave radiant fluxes by the green plants can be clearly observed. The human bodies and adjacent open areas no longer receive large amounts of strong long-wave radiation emitted by the sunlit ground area of Site A. These observations from thermal images provided preliminary evidences for the dependence of radiant fluxes, especially long-wave fluxes, on view factors of ambient objects or surfaces (Figure 6).

### Long-wave fluxes model

#### Long-wave model building

The results of the 15 fitted equations are displayed in Table 3. Based on the three aforementioned criteria, the model with all four predictors was selected as the final model of long-wave radiant fluxes in this study. The analysis of variance and the summary of the selected model are shown in Tables 4 and 5, respectively.

**Table 3.** Summary of all possible regression models for long-wave radiant fluxes.

Number of Predictors	Variables in the model				$R^2$	$R^2_a$	AIC	BIC
	SLVF	GNVF	SVF	$L_o$				
1	Y				0.2259	0.2136	580.82	587.34
1		Y			0.0687	0.0539	592.84	599.36
1			Y		0.0296	0.0142	595.51	602.03
1				Y	0.4690	0.4605	556.33	562.85
2	Y	Y			0.3143	0.2922	574.94	583.64
2	Y		Y		0.2443	0.2199	581.26	589.96
2	Y			Y	0.5653	0.5513	545.31	554.01
2		Y	Y		0.1267	0.0985	590.66	599.36
2		Y		Y	0.4800	0.4633	556.96	565.65
2			Y	Y	0.5535	0.5390	547.06	555.76
3	Y	Y	Y		0.3585	0.3269	572.61	583.49
3	Y	Y		Y	0.5879	0.5677	543.84	554.71
3	Y		Y	Y	0.6296	0.6114	536.91	547.78
3		Y	Y	Y	0.5819	0.5613	544.79	555.66
4	Y	Y	Y	Y	0.6706	0.6486	531.29	544.33

**Table 4.** The analysis of variance table for the long-wave model on view factors.

Long-wave model	df	Sum Sq	Mean Sq	F value	$p(>F)$
SLVF	1	7695.9	7695.9	41.1506	2.467E-08
GNVF	1	3010.2	3010.2	16.0959	.0001694
SVF	1	1504.1	1504.1	8.0424	.0062206
$L_o$	1	10,632.3	10,632.3	56.8513	2.992E-10
Regression	4	22,842.5	5710.6	30.5381	7.194E-14
Residual	60	11,221.1	187.0		
Total	64	34,063.6			

**Table 5.** Summary of regression equation of long-wave fluxes on view factors.

Predictor	Coefficient	S.E.	t	p	Significance	
					Level	Range
Constant	-69.275	75.060	-0.923	.3597	-	-
SLVF	116.585	29.002	4.020	.0002	.001	0.000–0.365
GnVF	-37.822	13.841	-2.733	.0082	.01	0.000–0.566
SVF	-122.865	31.668	-3.880	.0003	.001	0.054–0.340
$L_o$	1.169	0.155	7.540	.0000	.001	468.1–503.3

### Long-wave final model

The final model for long-wave radiant fluxes, L Model, was developed based on two major assumptions: (1) the relationship between the 5-min-averaged directional long-wave radiant fluxes  $L_i$ , measured as the irradiation on a surface, i.e. the sensor, and each view factor was linear; (2) such relationship could be expressed as a linear combination of view factors based on the physical understanding of radiative energy transfers within an enclosure. The L Model was highly statistically significant overall ( $p < .001$ ,  $N = 65$ ) and was obtained as:

$$L_i = -69.28 + 116.59 \text{ SLVF} - 37.82 \text{ GNVF} - 122.87 \text{ SVF} + 1.17 L_o, \quad (8)$$

with an adjusted  $R^2$  of 0.6486. This model explained around 65% of the sample variation in the measured directional long-wave fluxes within the open spaces surrounded by buildings.

In the model, the stronger directional long-wave radiant fluxes,  $L_i$ , could be attributed to a higher value of directional SLVF, a lower value of directional GNVF, a lower value of directional SVF, and a higher value of reference background long-wave fluxes  $L_o$ . All the predictors were highly significant in the model as shown in the t-test for each predictor ( $p < .01$ ,  $N = 65$ ).

The signs of the coefficient for the predictors, namely SLVF, GNVF, SVF, and  $L_o$ , were also reasonable: positive, negative, negative, and positive, respectively. The sunlit surfaces, represented by SLVF, were heated up by beam solar radiation to a higher surface temperature, and thus emitted more long-wave radiant fluxes than the non-sunlit ones. This explained the positive sign of the coefficient for SLVF. Meanwhile, the proximity to greenery (higher GNVF) and larger perceived sky views (higher SVF) were hypothesized to bring about cooling effects and reduce the incident long-wave radiant fluxes on the sensor surface. This justified the negative signs of the coefficients for GNVF and SVF. Also, the *reference background long-wave fluxes*  $L_o$ , representing the reference air temperature  $T_o$ , was significantly and positively linear to the measured directional long-wave fluxes  $L_i$ . The use of *reference background long-wave fluxes*  $L_o$  was to account for the seasonal changes in climatic conditions across the data collection period from early June to mid-October in 2015. This high significance of this predictor has showed its importance in adjusting or 'controlling' the different meteorological conditions.

### Short-wave fluxes model

#### Short-wave model building

The results of the 15 fitted equations are displayed in Table 6. Same as the long-wave fluxes model, the model with all four predictors was selected as the final model of short-wave radiant fluxes based on the three aforementioned criteria. The analysis of variance and the summary of the selected model are shown in Tables 7 and 8, respectively.

**Table 6.** Summary of all possible regression models for short-wave radiant fluxes.

Number of Predictors	Variables in the model				$R^2$	$R^2_a$	AIC	BIC
	SLVF	GNVF	SVF	$L_o$				
1	Y				0.1602	0.1462	546.37	552.75
1		Y			0.0051	-0.0115	556.88	563.26
1			Y		0.2615	0.2492	538.39	544.78
1				Y	0.1888	0.1753	544.22	550.60
2	Y	Y			0.1654	0.1371	547.98	556.49
2	Y		Y		0.4894	0.4721	517.51	526.02
2	Y			Y	0.2403	0.2145	542.15	550.66
2		Y	Y		0.3050	0.2814	536.63	545.14
2		Y		Y	0.1896	0.1621	546.16	554.67
2			Y	Y	0.5425	0.5269	510.71	519.22
3	Y	Y	Y		0.5414	0.5177	512.86	523.49
3	Y	Y		Y	0.2419	0.2027	544.02	554.65
3	Y		Y	Y	0.6156	0.5957	501.91	512.55
3		Y	Y	Y	0.5741	0.5520	508.27	518.91
4	Y	Y	Y	Y	0.6550	0.6308	497.21	509.98

**Table 7.** The analysis of variance table for the short-wave model on view factors.

Short-wave model	df	Sum Sq	Mean Sq	F value	$p(>F)$
SLVF	1	4222.0	4222.0	26.465	3.438E-06
GNVF	1	137.7	137.7	0.863	.3568
SVF	1	9909.2	9909.2	62.116	1.082E-10
$L_o$	1	2993.2	2993.2	18.763	6.068E-05
Regression	4	17,262.1	4315.5	27.057	1.325E-12
Residual	57	9093.1	159.5		
Total	61	26,355.2			

**Table 8.** Summary of regression equation of short-wave fluxes on view factors.

Predictor	Coefficient	S.E.	t	p	Significance	
					Level	Range
Constant	-32.620	7.471	-4.366	.0001	.001	—
SLVF	116.424	31.845	3.656	.0006	.001	0.000–0.365
GnVF	33.033	12.951	2.551	.0135	.05	0.000–0.566
SVF	248.295	30.057	8.261	.0000	.001	0.054–0.340
K <sub>o</sub>	0.134	0.031	4.332	.0001	.001	82.0–331.4

**Short-wave final model**

The final model for short-wave radiant fluxes, K Model, was obtained in the same way as the L Model. The K Model was highly

significant overall ( $p < .001$ ,  $N = 62$ ) and can be expressed as:

$$K_i = -32.62 + 116.42 \text{ SLVF} + 33.03 \text{ GnVF} + 248.30 \text{ SVF} + 0.13 \text{ K}_o \tag{9}$$

with an adjusted  $R^2$  of 0.6308. This model explained around 63% of the sample variation in the measured directional short-wave fluxes within the open spaces surrounded by buildings.

In the model, the stronger directional short-wave radiant fluxes,  $K_i$ , could be attributed to a higher value of directional

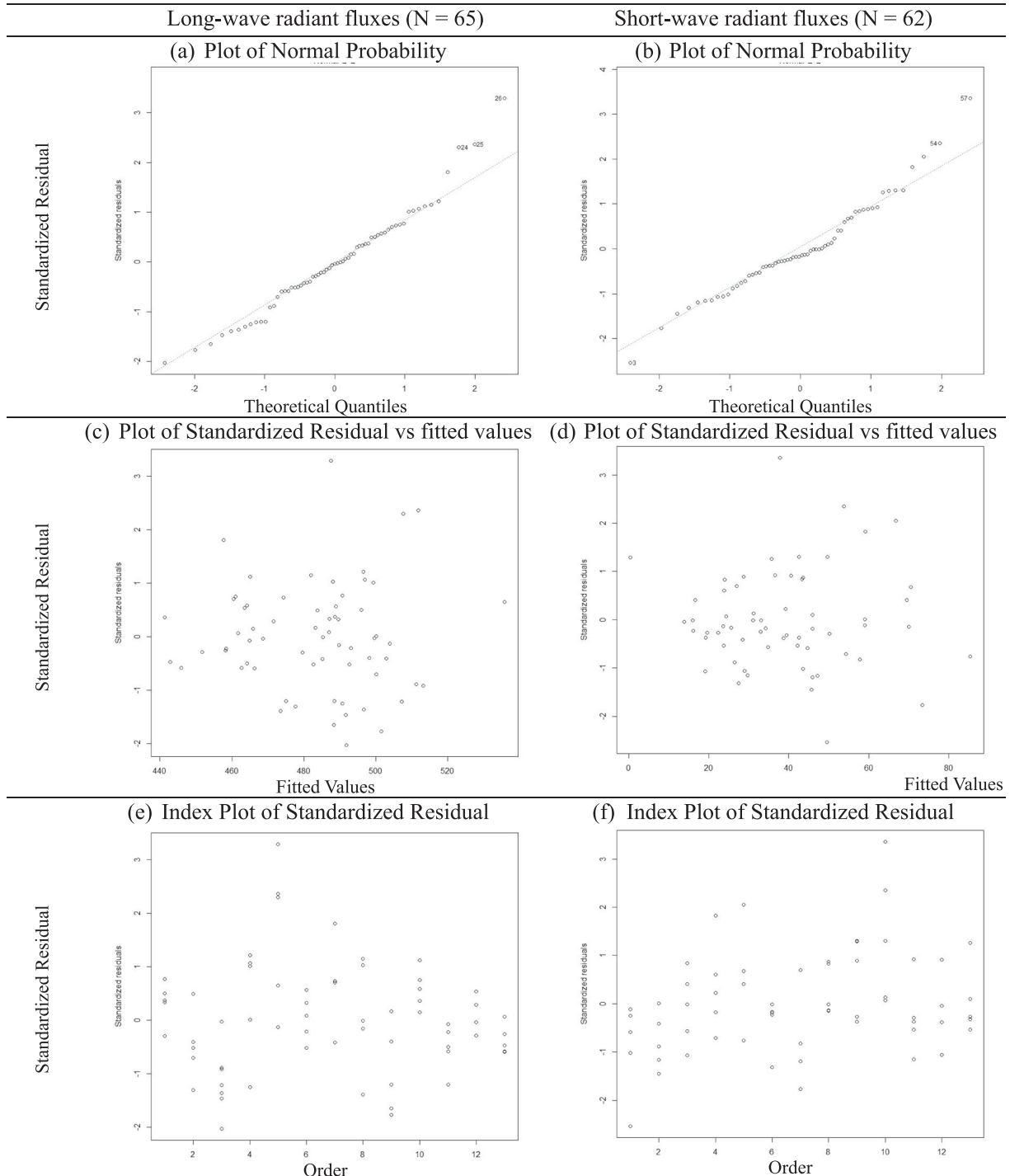


**Figure 7.** Plots of standardized residuals.

SLVF, a higher value of directional GNVF, a higher value of directional SVF, and higher value of reference diffuse sky radiation  $K_o$ . All the predictors were highly significant in the model as shown in the  $t$ -test for each predictor ( $p < .001$ ,  $N = 62$ ), except for the  $t$ -test of GNVF with significance level of only 0.05.

The signs of the coefficient for the predictors, namely SLVF, GNVF, SVF, and  $K_o$ , were all positive. The positive sign of the coefficient for SLVF could be explained by the higher amount of solar radiation (including short-wave fluxes) falling incident on, and thus reflected by, the sunlit surface than its counterpart. The larger perceived sky view (higher SVF) acted as the source of diffuse (short-wave) radiation scattered by the sky (atmosphere). This justified the positive sign of the coefficient for SVF in the model.

The coefficient for GNVF was also significant and positive. First of all, the predictor GNVF was highly significant in the model for short-wave fluxes as its  $t$ -test was highly significant ( $p < .05$ ,  $N = 62$ ). In other words, the variations in GNVF could, at least statistically, explain some of the variations in short-wave radiant fluxes  $K_i$ . Secondly, a possible reason for the positive contribution of GNVF could be the reflected solar radiation from the leaves, and/or the transmitted diffuse sky radiation through the gaps between leaves. Owing to the low surface temperature of

around 300 K, terrestrial surfaces, including greenery surface, in the built environment could not emit a large amount of short-wave fluxes according to the Planck's law. Therefore, the variations in short-wave radiant fluxes incident on the sensors from the built environment could only be attributed to reflected solar radiation from sunlit or reflective surfaces, and diffuse sky radiation from the atmosphere, but not to the solar beam radiation as the sensors were not directly sunlit. The greenery features could provide not only some reflective surfaces (leaves) for solar radiation but also gaps between the leaves for diffuse sky radiation to pass through and reach the sensor. Besides SLVF and SVF, these might be the physical contributions of GNVF to the variations in short-wave radiant fluxes  $K_i$  within the built environment.

The diffuse solar radiation,  $K_o$ , obtained from the Kau Sai Chau (KSC) Automatic Weather Station of Hong Kong Observatory was also positively linear to the directional short-wave radiant fluxes,  $K_i$ . As in the long-wave model, the short-wave model included the fourth predictor, the diffuse sky radiation  $K_o$ , in order to adjust for different meteorological conditions. This predictor was also highly significant in the model as proved by the  $t$ -test. This justified the use of the diffuse solar radiation as background information to 'control' the different weather conditions of the day in the regression model.

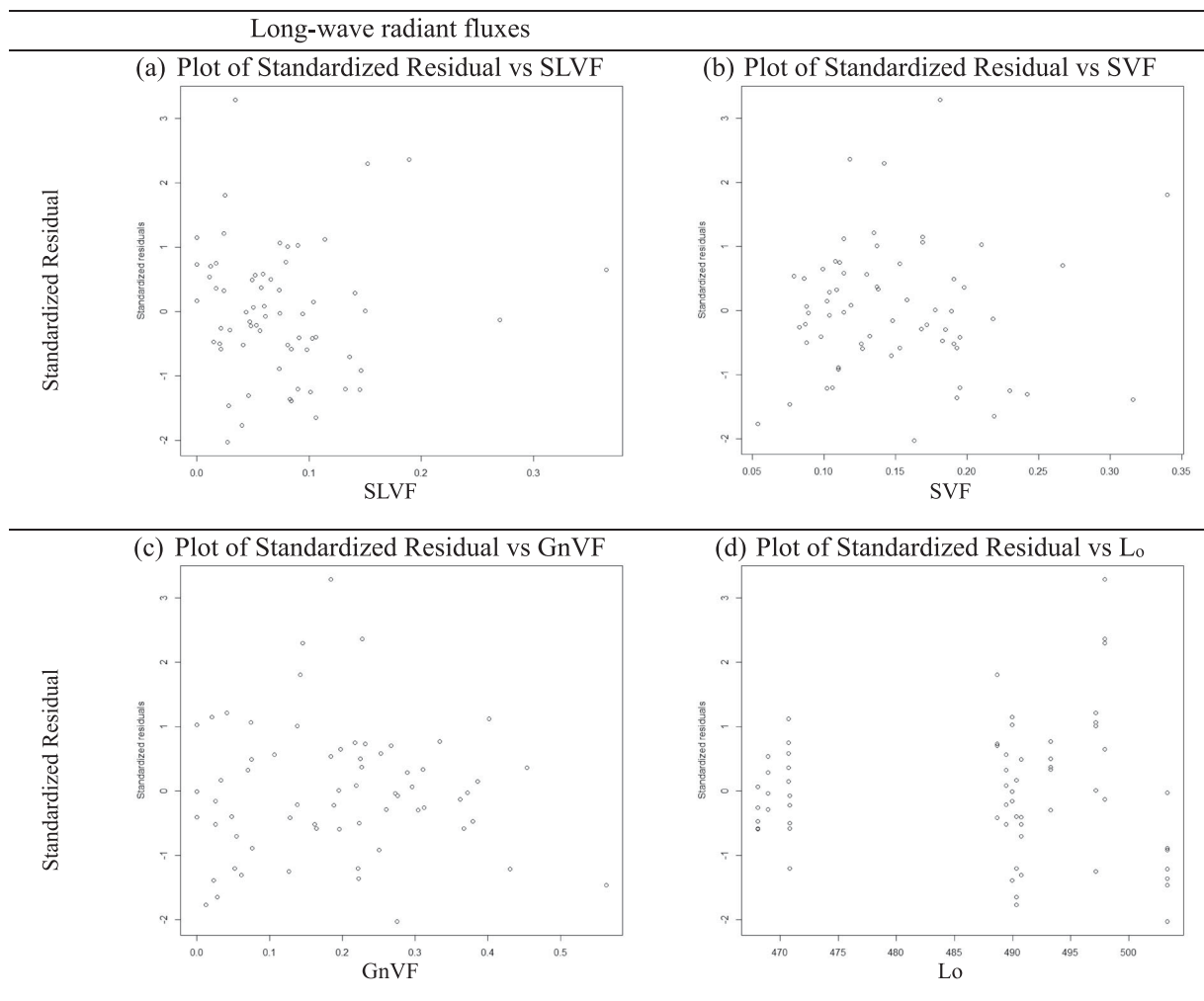


Figure 8. Plots of standardized residuals.

### Models checking: residual analysis

The two basic assumptions applied in the regression analysis were as follows:

- I. The errors are normally distributed with mean zero and constant variance.
- II. The errors are uncorrelated, or equivalently, all pairs of errors are independent.

#### Plot of normal probability

If errors are normally distributed, then approximately 95% of the standardized residuals should fall between  $-2$  and  $+2$ . Referring to Figure 7(a and b), only 3 out of 65 long-wave data points (4.6%) are outside this range, and 3 out of 62 short-wave data points (4.8%) are outside this range. Also, the plots display approximately straight lines, showing no obvious violation of the normality assumption.

#### Plot of standardized residuals against fitted values

The plots in Figure 7(c and d) showed no obvious trend of linearity, non-linearity, double bow, and inward or outward megaphone. Most of the standardized residuals, approximately

95% of the data, are within the range of  $-2$  and  $+2$ . The plots thus show no obvious violation of the assumptions of mean zero and constant variance.

#### Index plot of standardized residuals

Figure 7(e and f) also showed no obvious trend of linearity, non-linearity, double bow, and inward or outward megaphone. Most of the standardized residuals, approximately 95% of the data, fall between the range of  $-2$  and  $+2$ . The plots thus show no obvious violation of independent assumptions over order of measurements even if at the same site.

#### Plot of standardized residuals against independent variables

Figures 8 and 9 are the plots of standard residuals against the independent variables for the long-wave and short-wave models, respectively. The plots show no obvious trend of linearity, non-linearity, double bow, and inward or outward megaphone. Most of the standardized residuals, approximately 95% of the data, are within the range of  $-2$  and  $+2$ . The plots thus show no obvious violation of the assumptions of mean zero and constant variance for each independent variable.

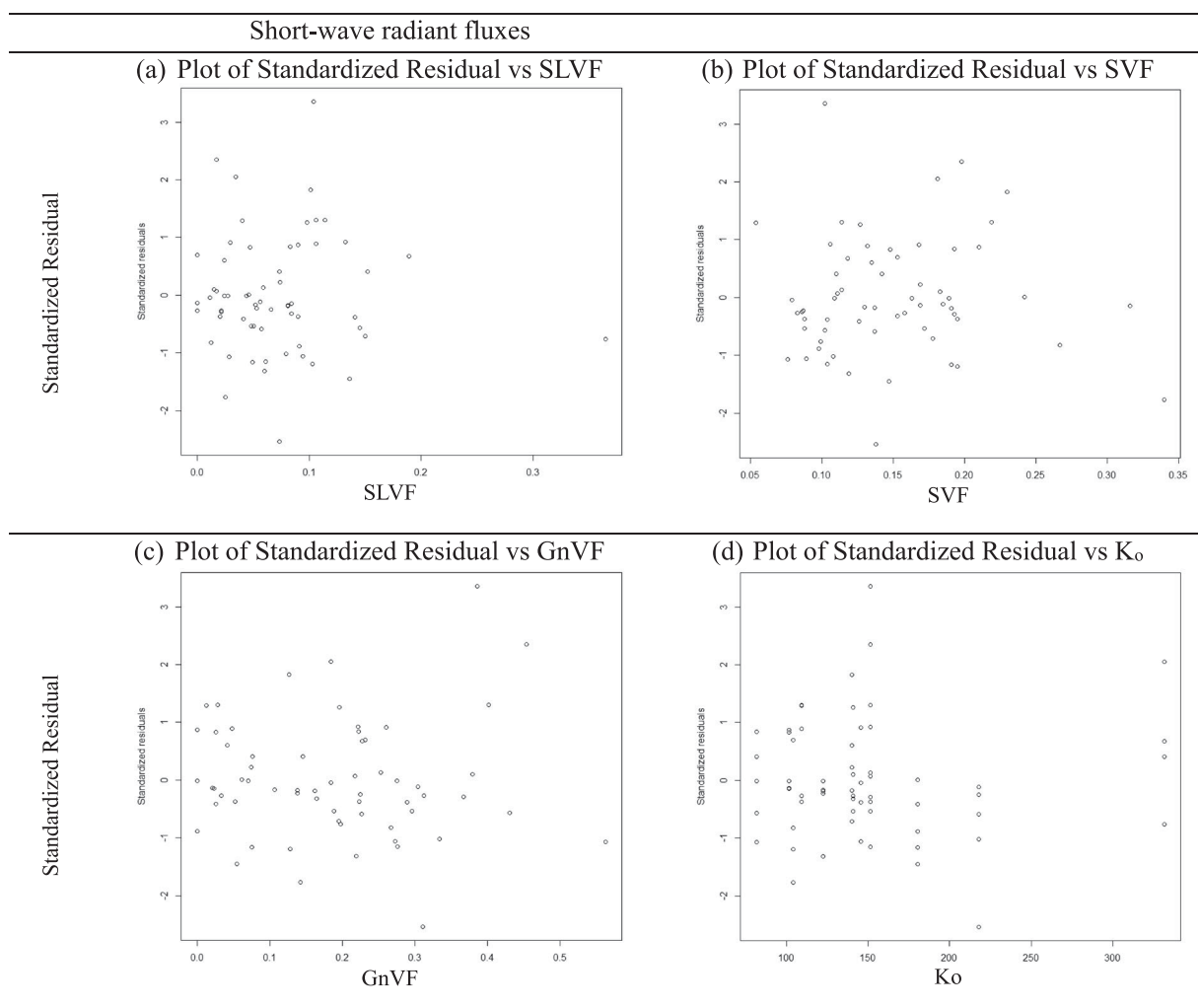


Figure 9. Plots of standardized residuals.

**Table 9.** The correlation matrix for long-wave model ( $N = 65$ ).

	$L_i$	SLVF	GNVF	SVF	$L_o$
$L_i$	1.000	0.475	-0.262	-0.172	0.685
SLVF		1.000	0.072	-0.078	0.256
GNVF			1.000	-0.236	-0.233
SVF				1.000	0.167
$L_o$					1.000

**Table 10.** The correlation matrix for short-wave model ( $N = 62$ ).

	$L_i$	SLVF	GNVF	SVF	$L_o$
$K_i$	1.000	0.400	0.071	0.511	0.434
SLVF		1.000	-0.003	-0.141	0.457
GNVF			1.000	-0.255	0.099
SVF				1.000	-0.171
$K_o$					1.000

### Correlation matrix

The correlation matrices among the predictors for the long-wave and short-wave models are shown in Tables 9 and 10, respectively. The intercorrelations between predictors obtained are low. None of the correlations between any two of the predictors are near unity. Since none of the pairwise correlations are large, there exists no indication of the near linear dependency among the predictors in each model.

### Discussion

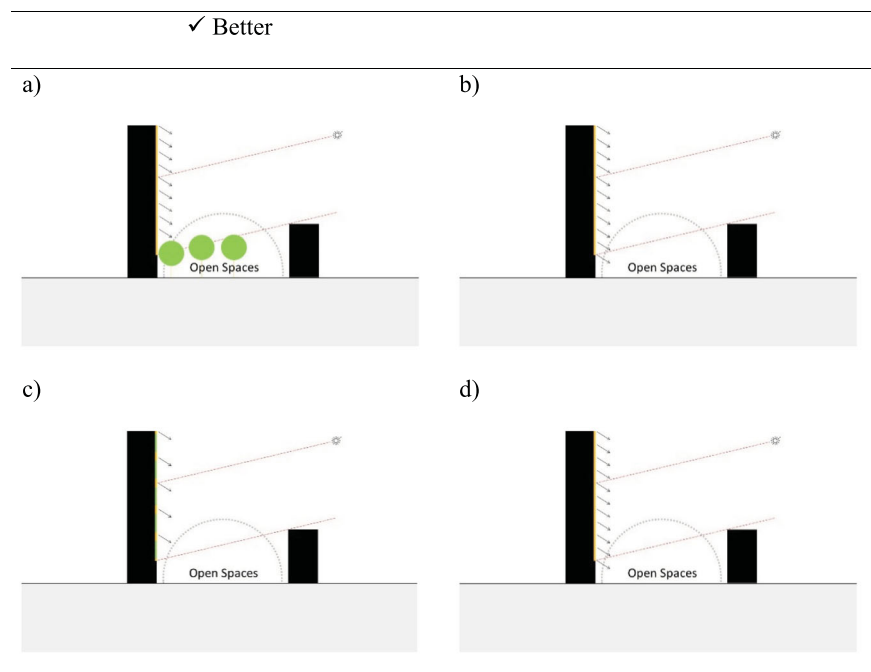
This study examined the empirical and causal relationships between different view factors and radiant fluxes. In order to draw causal inference from this observational study, the key was to make use of the theoretical relationship between dependent and independent variables in the regression equation (Freeman 2005). The theoretical relationship and the result of regression analysis can be summarized as follows:

### Relationship between view factors and radiant fluxes

Based on the theory of radiative energy transfer, the radiant fluxes on a surface, e.g. a sensor, can be expressed as a linear combination of view factors within an enclosure formed by a built environment. This study thus examined the linear dependence of radiant fluxes on view factors, namely SLVF, GNVF, and SVF. SLVF represents the sunlit built environment that might reflect more short-wave fluxes and emit more long-wave fluxes due to more irradiation from the sun. GNVF represents the greenery feature in the built environment that might absorb certain portions of solar radiation for photosynthesis and emit fewer long-wave fluxes due to its water content of higher specific heat capacity. SVF represents the visible sky that might scatter solar radiation and emit fewer long-wave fluxes due to lower effective temperature. These view factors are casted by the built environment, for example the urban morphology and building envelope, and thus can be regarded as indicators of the effect of the thermal built environment on existing radiant fluxes. Therefore, the use of multiple linear regression analysis is justified for the study of the empirical and causal relations between radiant fluxes and the built environment.

### Discussion on linear regression analysis

The regression models for both long-wave and short-wave explained 65% and 63% of the sample variations in radiant fluxes. The results showed that nearly two-thirds of variations in directional radiant fluxes, both long-wave and short-wave, could be attributed to the effects of SLVF, GNVF, SVF, and the background meteorological conditions. The signs of regression coefficients for the predictors were reasonable. The predictors were all highly significant in the regression equations. These reaffirmed the use of these predictors in the regression models.

**Figure 10.** Tall trees or vertical greening should be considered for better cooling effect of open space.

## Conclusions and further work

To sum up, by using only four simple predictors, the models in the study, with an adjusted  $R^2$  of at least 63%, were able to explain nearly two-thirds of variations in the radiant fluxes measured from the outdoor field measurements. Given the objective of the study was to identify and evaluate any empirical relation between radiant fluxes and the view factors casted by the built environment, the obtained models did achieve to identify and explain their significant linear correlations with radiant fluxes. Nevertheless, future work is certainly needed to improve the predicting power of the models and to provide a more comprehensive description of the built environment using other view factors.

## Implications for urban planning

Based on the current findings, relevant recommendations on environmental urban planning for Hong Kong, one of the high-density cities in hot and humid regions, could be provided, but not limited to the following:

- To avoid overheating, especially in the afternoons during summer, outdoor or public spaces should be shaded by the surrounding buildings if direct sunlight can reach the ground of that outdoor space.
- If the outdoor space is already adequately shaded from direct sunlight, then the next measure is to maximize the sky view for optimizing the radiative cooling effect of the sky on pedestrian level.
- Greenery features within the built environment could reduce the short-wave radiant fluxes approaching the outdoor spaces, and thus alleviate the potential increases in intra-urban temperature and outdoor MRT. For example, tall trees with wide and dense canopies could absorb some solar radiation and reduce the amount of short-wave radiant fluxes reaching the open spaces (see Figure 10(a)). Similarly, vertical greening on building envelopes could absorb some solar radiation and reflect less short-wave fluxes towards the open space, particularly when compared to sunlit building façades made of concrete (see Figure 10(c)).

## Acknowledgements

The authors are thankful to Mr Julian Lee and Ms Judy Zhang for their effort and kind help. The authors also cordially thank Mr Max Lee for setting up the equipment.

## Disclosure statement

No potential conflict of interest was reported by the authors.

## Funding

The research is made possible with financial support from the Construction Industry Council (CIC) on the project 'A Study of Impact of Building Envelope on Urban Outdoor Thermal Environment' (Project ID: CICR/04/13) ([http://www.cic.hk/eng/main/research\\_data\\_analytics/\\_cic\\_fund\\_projects/](http://www.cic.hk/eng/main/research_data_analytics/_cic_fund_projects/)).

## References

- ASHRAE. 2013. *ASHRAE Fundamentals Handbook 2013*. SI ed. American Society of Heating, Refrigerating, and Air-Conditioning Engineers. ISBN: 978-1936504466.
- Butcher, K. 1999. *CIBSE Guide. A, Environmental Design*. 6th ed. London: Chartered Institution of Building Services Engineers.
- Chapman, L., J. E. Thornes, and A. V. Bradley. 2001. "Rapid Determination of Canyon Geometry Parameters for Use in Surface Radiation Budgets." *Theoretical and Applied Climatology* 69: 81–89.
- Çengel, Y. A. 2003. *Heat Transfer: A Practical Approach*. 2nd ed. Boston, MA: McGraw-Hill.
- Erell, E., D. Pearlmutter, and T. Williamson. 2010. *Urban Microclimate: Designing the Spaces Between Buildings*. 1st ed. London: Routledge.
- Fanger, P. O. 1972. *Thermal Comfort*. New York: McGraw-Hill.
- Freeman, D. A. 2009. *Statistical Models: Theory and Practice*. 1st ed. Cambridge: Cambridge University Press.
- Hakim, A. A., H. Petrovitch, C. M. Burchfiel, G. W. Ross, B. L. Rodriguez, L. R. White, et al. 1998. "Effects of Walking on Mortality Among Non-Smoking Retired Men." *The New England Journal of Medicine* 338: 94–99.
- Hamdi, R., and G. Schayes. 2007. "Sensitivity Study of the Urban Heat Island Intensity to Urban Characteristics." *International Journal of Climatology* 28: 973–982.
- Howell, J. R., M. P. Menguc, and R. Siegel. 2010. *Thermal Radiation Heat Transfer*. 5th ed. Boca Raton, FL: CRC Press.
- Höppe, P. 1999. "The Physiological Equivalence Temperature – A Universal Index for the Biometeorological Assessment of the Thermal Environment." *International Journal of Biometeorology* 43 (2): 71–75.
- Jendritzky, G., R. de Dear, and G. Havenith. 2012. "UTCI – Why Another Thermal Index?" *International Journal of Biometeorology* 56: 421–428.
- Johnson, G. T., and J. D. Watson. 1984. "The Determination of View-Factors in Urban Canyons." *Journal of Climate and Applied Meteorology* 23: 329–335.
- Krüger, E. L., F. O. Minella, and F. Rasia. 2011. "Impact of Urban Geometry on Outdoor Thermal Comfort and Air Quality from Field Measurements in Curitiba, Brazil." *Building and Environment* 46: 621–634.
- Lai, A., M. J. Maing, and E. Ng. 2017. "Observational Studies of Mean Radiant Temperature Across Different Outdoor Spaces Under Shaded Conditions in Densely Built Environment." *Building and Environment* 114: 397–409.
- Lee, H., Mayer, H., and Schindler, D. 2014. "Importance of 3-D Radiant Flux Densities for Outdoor Thermal Comfort on Clear-Sky Summer Days in Freiburg, Southwest Germany." *Meteorologische Zeitschrift*. doi:10.1127/0941-2948/2014/0536.
- Lin, T. P., A. Matzarakis, and R. L. Hwang. 2010. "Shading Effect on Long-Term Outdoor Thermal Comfort." *Building and Environment* 45: 213–221.
- Lin, T. P., K. T. Tsai, R. L. Hwang, and A. Matzarakis. 2012. "A Quantification of the Effect of Thermal Indices and Sky View Factor on Park Attendance." *Landscape and Urban Planning* 107: 137–146.
- Mbiok, A., and R. Weber. 2000. *Radiation in Enclosures: Elliptic Boundary Value Problem*. Berlin: Springer.
- Michael, F. M. 2013. *Radiative Heat Transfer*. 3rd ed. Cambridge: Academic Press.
- Montgomery, D. C., and E. A. Peck. 1982. *Introduction to Linear Regression Analysis*. New York: Wiley.
- Oke, T. R. 1988. "Street Design and Urban Canopy Layer Climate." *Energy and Buildings* 11: 103–113.
- Pardoe, I. 2012. *Applied Regression Modeling*. 2nd ed. Hoboken, NJ: Wiley.
- Rathore, M. M., and R. R. A. Kapuno. 2011. *Engineering Heat Transfer*. 2nd ed. Sudbury, MA: Jones & Bartlett Learning.
- Sakamoto, Y., M. Ishiguro, and G. Kitagawa. 1987. *Akaike Information Criterion Statistics*. Dordrecht: Reidel.
- Schwarz, G. 1978. "Estimating the Dimension of a Model." *The Annals of Statistics* 6: 461–464.
- Steyn, D. G. 1980. "The Calculation of View Factors from Fish-Eye Lens Photographs." *Atmosphere-Ocean* 18: 254–258.
- Tan, C. L., N. H. Wong, and S. K. Jusuf. 2013. "Outdoor Mean Radiant Temperature Estimation in the Tropical Urban Environment." *Building and Environment* 64: 118–129.

- Thorsson, S., F. Lindberg, I. Eliasson, and B. Holmer. 2007. "Different Methods for Estimating the Mean Radiant Temperature in an Outdoor Urban Setting." *International Journal of Climatology* 27: 1983–1993.
- Unger, J. 2009. "Connection Between Urban Heat Island and Sky View Factor Approximated by a Software Tool on a 3D Urban Database." *International Journal of Environment and Pollution* 36 (1/2/3): 59–80.
- Watson, I. D., and G. T. Johnson. 1987. "Graphical Estimation of Sky View-Factors in Urban Environments." *Journal of Climatology* 7: 193–197.
- Wong, N. H., and S. K. Jusuf. 2010. "Air Temperature Distribution and the Influence of Sky View Factor in a Green Singapore Estate." *Journal of Urban Planning and Development* 136: 261–272.